

Shape determination of 3-D reinforcement corrosion in concrete based on observed temperature on concrete surface

Takahiko Kurahashi[†]

*Department of Mechanical Engineering, Nagaoka University of Technology,
1603-1 Kamitomioka-cho, Nagaoka-shi, Niigata, 940-2188, Japan*

Hideki Oshita[‡]

*Department of Civil Engineering, Chuo University, 1-13-27 Kasuga, Bunkyo-ku,
Tokyo, 112-8551, Japan*

(Received July 26, 2009, Accepted January 20, 2010)

Abstract We present the shape determination method of 3-D reinforcement corrosion based on observed temperature on concrete surface. The non-destructive testing for reinforcement corrosion in concrete using a heat image on concrete surface have been proposed by Oshita. The position of the reinforcement of corrosion or the cavity can be found using that method. However, the size of those defects can not be precisely measured based on the heat image. We therefore proposed the numerical determination system of the shape for the reinforcement corrosion using the observed temperature on the concrete surface. The adjoint variable method is introduced to formulate the shape determination problem, and the finite element method is employed to simulate the heat transfer problem. Some numerical experiments and the examination for the number of the observation points are shown in this paper.

Keywords: reinforcement corrosion; observed temperature on concrete surface; shape determination problem; adjoint variable method; finite element method.

1. Introduction

In recent years, the importance for the maintenance of the concrete structure increases, and several non-destructive testing are applied to the concrete structure to evaluate whether the safety standard is satisfied. As one of the testing, a method of the non-destructive testing using the heat image on the concrete surface has been developed by the research grope of Oshita (Taniguchi and Oshita 2008). Appling this method to the concrete structure, the position of the reinforcement of the corrosion or the cavity can be confirmed by the heat image (See section 2). However, there is a disadvantage that the magnitude of those defects can not be numerically evaluated.

The inverse scattering method (Bostock 2002, Khalaj-Amirhosseini *et al.* 2007) is enumerated as one of the method that is used to obtain the unknown shape of the defect. If this method is applied

[†] Ph.D., Corresponding author, E-mail: kurahashi@mech.nagaokaut.ac.jp

[‡] Professor, E-mail: oshita@civil.chuo-u.ac.jp

to evaluate the unknown shape of the defect, the unknown shape can be approximately expressed by the difference of the physical constants. In addition, the adjoint variable and the sensitivity equation methods can be also applied to evaluate the state of the defect. The sensitivity equation and the adjoint variable methods are the deterministic approach, and these methods are frequently used to solve the inverse problems, i.e., the boundary control problems (He *et al.* 1998, Gunzburger *et al.* 1998), the parameter identification problems (Kreible *et al.* 2007), the initial value determination problems (Dimet *et al.* 2002). In these problems, a performance function expressed by the square sum of the residual between the computed and the target state values is defined, and the unknown parameter is obtained by solving the minimization problem of the performance function. In case that the sensitivity equation method is applied to the inverse problem, the sensitivity equations expressed by the derivative of the state equation with respect to the unknown parameters should be solved to obtain the unknown parameters. If there are a lot of the unknown parameters in the inverse problem, it takes much computational time to compute the unknown parameters, because a lot of sensitivity equations should be solved. On the other hand, if the adjoint variable method is applied to solve the inverse problem, the adjoint equation is solved to obtain the unknown adjoint variables. In case of the adjoint variable method, the number of the adjoint equation does not depend on the number of the unknown parameters. Therefore, it does not take much computational time comparing with the case of the sensitivity equation method, and it appears that the adjoint variable method is suitable for the inverse problem included a lot of unknown parameters. In this study, the unknown parameters are the coordinate values on the surface of the reinforcement corrosion in the concrete, and a lot of unknown parameters should be employed to evaluate the unknown corrosion shape. Therefore, the adjoint variable method is applied to evaluate the shape of the unknown corrosion shape in this study. The researches for the numerical shape determination system based on the adjoint variable method have been carried out. In the flow problem, Pironneau found out the optimal shape that minimizes the drag force (Pironneau 1973, 1974). The research groupe of Kawahara investigates the shape optimization problem using the finite element method using the stabilized bubble function element (Ogawa *et al.* 2003, Yagi *et al.* 2007). In addition, if it is seen that there is oscillation on the surface of the computed shape, it is said that the oscillation can be controlled by the traction method (Azegami *et al.* 2006) or the method suggested by Jameson (Jameson 2003).

In addition, there are two types methods to solve the shape determination problem. One method is refer to as the topology optimization procedure (Luo *et al.* 2008, Challis *et al.* 2009), the other method is refer to as the shape optimization procedure (Pironneau 1973, 1974, Jameson 2003, Ogawa *et al.* 2003, Azegami *et al.* 2006, Yagi *et al.* 2007). In the topology optimization procedure, the shape of the structure is expressed by the level set function, and this procedure is applied to the structural design problem (Luo *et al.* 2008) and the topology optimization problem in the flow field (Challis *et al.* 2009). If this procedure is applied to the shape determination problem, the shape of the target body is not specifically determined but is approximately determined. Because the shape is expressed by the level set function, and the boundary of the shape is expressed as the gray zone. On the other hand, if the shape optimization procedure is applied to the problem that the unknown shape is determined, the shape is specifically expressed by the information of the nodal coordinates. Therefore we focused on the shape optimization technique to obtain the unknown corrosion shape in this study.

For the 2D corrosion shape determination problem based on the temperature on the concrete

surface, the evaluation system using the adjoint variable and the finite element methods has been examined, and a problem in the present method was clarified. The problem is that if this system is applied to the concrete with the partially reinforcement corrosion, the thickness of the reinforcement corrosion can not be precisely evaluated. If this system is applied to the problem of the partial reinforcement corrosion, it is necessary to extend this system to the 3-D problem. Therefore, we examine this system extended to the 3-D problem in this study. The state equation and the formulation based on the adjoint variable method are shown in the sections 3 and 4. The finite element method is applied to compute the heat transfer field. In the computation of 3D problem, it takes a lot of storage requirement and computational time to obtain the solution. In this study, the element-by-element conjugate gradient method is applied to solve the finite element equation. For the computation of the shape optimization, an iterative procedure is introduced in section 4, and results obtained by numerical experiments are shown in section 5. Finally, the conclusions of this study are described in the section 6.

2. Observation system of temperature on concrete surface

A method of the non-destructive testing for the reinforcement corrosion in concrete have been proposed by Oshita *et al.* (Taniguchi and Oshita 2008) (Fig. 1). This method is that position of reinforcement corrosion or cavity can be investigated by using the heat image on the concrete surface (Figs. 2 and 3). The flow of this testing is shown as follows.

1. Heat a coil on concrete surface. Heat reinforcement bars by electromagnetic induction.
2. After the heating, except the coil and observe heat image by infrared sensor.

The advantage of this testing is to find the position of reinforcement corrosion or cavity easily. However, the depth and the magnitude for those defects can not be numerically evaluated. Therefore we develop the numerical shape determination system for the reinforcement of the corrosion in concrete using the observed temperature on concrete surface.

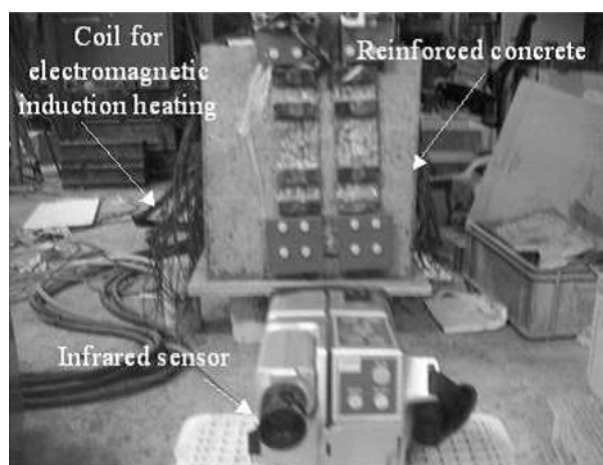


Fig. 1 System of non-destructive testing

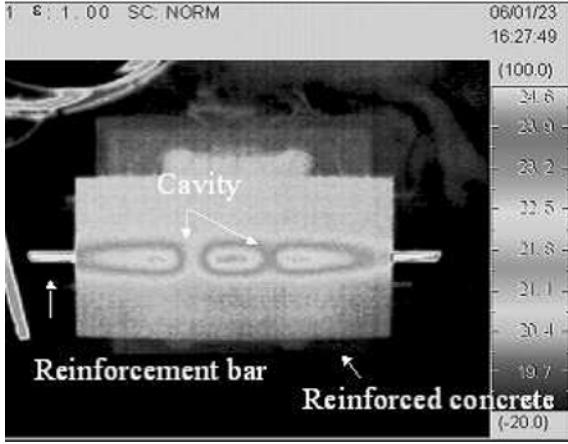


Fig. 2 Heat image (1) : Cavity

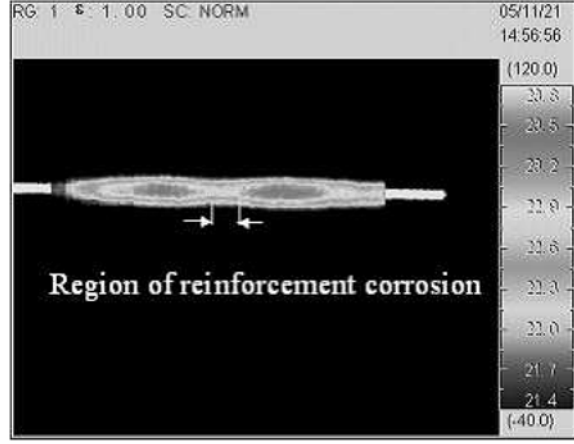


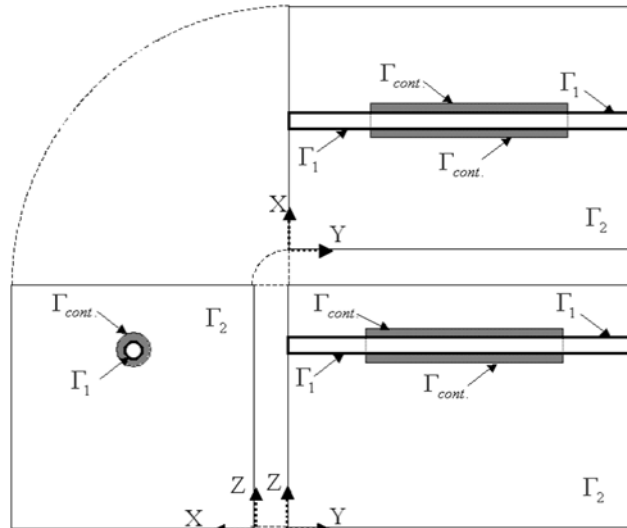
Fig. 3 Heat image (2) : Reinforcement corrosion

3. State equation, initial and boundary conditions

To simulate of the heat transfer field, the heat transfer equation is employed. The heat transfer equation is defined in the three dimensional space $\Omega \in R^3$ with the boundary Γ shown in Fig. 4, and is written as

$$\rho c \dot{\phi} - \kappa \phi_{,ii} = 0 \tag{1}$$

where ρ , c , κ and ϕ indicate the density, the specific heat, the thermal conductivity and the temperature. Initial and boundary conditions are defined as



Γ_2 : Boundary for concrete surface

Fig. 4 Diagram of computational domain and boundaries

$$\begin{aligned}\phi(t_0) &= \hat{\phi}_0 \quad \text{in } \Omega \\ \phi &= \hat{\phi} \quad \text{on } \Gamma_1 \\ q &= \kappa\phi, n_i = \hat{q} \quad \text{on } \Gamma_2\end{aligned}$$

where Ω , Γ_1 and Γ_2 indicate the computational domain, the Dirichlet boundary and the Neumann boundary, and q denotes the heat flux. In addition, Γ_{cont} indicates the surface boundary for the reinforcement corrosion. Applying the finite element method to the Eq. (1), the finite element equation for each element is obtained as

$$\rho_e c_e [M_e] \{\dot{\phi}_e\} + \kappa_e [H_e] \{\phi_e\} = \{T_e\}, \quad \text{in } \Omega_e \quad (3)$$

where the matrices $[M_e]$, $[H_e]$ and the vectors $\{\phi_e\}$, $\{T_e\}$ indicate the mass and the heat transfer matrices and the temperature at the each nodes for the tetrahedron element and the heat flux vector. Assembling the finite element equations for each element, the superposed finite element equation is written as

$$[A] \{\dot{\phi}\} + [B] \{\phi\} = \{C\}, \quad \text{in } \Omega \quad (4)$$

where the matrices $[A]$, $[B]$ and the vector $\{C\}$ indicate $\sum_{e=1}^{mx} \rho_e c_e [M_e]$, $\sum_{e=1}^{mx} \kappa_e [H_e]$ and $\sum_{e=1}^{mx} \{T_e\}$, and mx is the total number of elements.

4. Formulation for shape determination problem

The shape of the reinforcement corrosion is determined by solving the minimization problem of a functional. In this study, the functional is defined by the square sum of the residual between the computed and observed temperature on the concrete surface. The functional is written as

$$J = \frac{1}{2} \int_{t_0}^{t_f} \{\phi - \phi_{obs.}\}^T [R] \{\phi - \phi_{obs.}\} dt \quad (5)$$

where $[R]$, ϕ and $\phi_{obs.}$ denote the weighting diagonal matrix, the computed temperature and the observed temperature. The functional is called the performance function and minimizing the performance function mean that the computed temperature on the concrete surface is close to the observed temperature. The temperature ϕ is obtained by computing the heat transfer equation, and that equation is introduced as the constraint condition for the performance function. In addition, the computational conditions, i.e., the initial and boundary condition for the state equation, are also employed as the constraint conditions. By introducing the Lagrange multiplier for minimization of the performance function with the constraint conditions, Eqs. (2) and (4), the Lagrange function is defined as

$$J^* = J - \int_{t_0}^{t_f} \{\lambda\}^T ([A] \{\dot{\phi}\} + [B] \{\phi\} - \{C\}) dt \quad (6)$$

where λ indicates the Lagrange multiplier. In addition, the design variables are the nodal coordinates x_i on the surface of the corrosion, and those variables are included in the coefficient matrices $[A]$, $[B]$ and $[C]$ of the finite element equation. To obtain the stationary condition of the Lagrange function, the first variation of the Lagrange function is calculated. Consequently, the following equation is obtained:

$$\begin{aligned}
\delta J^* &= \int_{t_0}^{t_f} \left(\{ \delta \lambda \}^T \left\{ \frac{\partial J^*}{\partial \lambda} \right\} + \left\{ \frac{\partial J^*}{\partial \phi} \right\} \{ \delta \phi \} + \left\{ \frac{\partial J^*}{\partial C} \right\}^T \{ \delta C \} \right) dt + \{ \delta x_i \}^T \left\{ \int_{t_0}^{t_f} \frac{\partial J^*}{\partial x_i} dt \right\} \\
&= \int_{t_0}^{t_f} \left(\{ \delta \lambda \}^T (-[A] \{ \dot{\phi} \} - [B] \{ \phi \} + \{ C \}) \right. \\
&\quad \left. + (\{ \dot{\lambda} \}^T [A] - \{ \lambda \}^T [B] + \{ \phi - \phi_{obs.} \}^T [R]) \{ \delta \phi \} + \{ \lambda \}^T \{ \delta C \} \right) dt \\
&\quad \left. + \{ \lambda(t_f) \}^T \{ \delta \phi(t_f) \} - \{ \lambda(t_0) \}^T \{ \delta \phi(t_0) \} + \{ \delta x_i \}^T \left\{ \int_{t_0}^{t_f} \frac{\partial J^*}{\partial x_i} dt \right\} \right)
\end{aligned} \tag{7}$$

As the gradient vectors, the following equations are obtained. The gradient of the Lagrange function with respect to the Lagrange multiplier means the state equation, and is written as

$$\left\{ \frac{\partial J^*}{\partial \lambda} \right\} = -[A] \{ \dot{\phi} \} - [B] \{ \phi \} + \{ C \} = -([A] \{ \dot{\phi} \} + [B] \{ \phi \} - \{ C \}) = \{ 0 \}. \quad \text{in } \Omega \quad t \in [t_0, t_f] \tag{8}$$

In addition, the gradient of the Lagrange function with respect to the state variable means the equation of the Lagrange multiplier, and is derived as

$$\left\{ \frac{\partial J^*}{\partial \phi} \right\} = [A]^T [\dot{\lambda}] - [B]^T \{ \lambda \} + [R]^T \{ \phi - \phi_{obs.} \} = \{ S \}. \quad \text{in } \Omega \quad t \in [t_0, t_f] \tag{9}$$

Considering the initial and boundary conditions for state variable Eq. (2), the $\rho_e c_e$ terminal and the boundary conditions for the Lagrange multiplier are obtained as

$$\begin{aligned}
\lambda(t_f) &= 0 \quad \text{in } \Omega \\
\lambda &= 0 \quad \text{on } \Gamma_1 \\
s &= 0 \quad \text{on } \Gamma_2
\end{aligned} \tag{10}$$

The full implicit scheme is employed as the temporal discretization technique for the heat transfer and the adjoint equations. To solve the finite element equations for the state and the adjoint equations, the element-by-element conjugate gradient method is employed.

Moreover, the gradient of the Lagrange function with respect to the nodal coordinates is obtained as

$$\left\{ \int_{t_0}^{t_f} \frac{\partial J^*}{\partial x_i} dt \right\} = \left\{ \int_{t_0}^{t_f} \{ \lambda \}^T \left(\left[\frac{\partial A}{\partial x_i} \right] \{ \dot{\phi} \} + \left[\frac{\partial B}{\partial x_i} \right] \{ \phi \} - \left[\frac{\partial C}{\partial x_i} \right] \right) dt \right\} \quad \text{in } \Omega \tag{11}$$

and this gradient is obtained by the computed temperature and the Lagrange multiplier. Here, the matrices $\left[\frac{\partial A}{\partial x} \right]$, $\left[\frac{\partial B}{\partial x} \right]$ and the vector $\left\{ \frac{\partial C}{\partial x} \right\}$ indicate $\Sigma_{i-1}^{m_x} \rho_i c_i \left[\frac{\partial M_i}{\partial x_i} \right]$, $\Sigma_{i-1}^{m_x} \kappa_i \left[\frac{\partial H_i}{\partial x_i} \right]$ and $\Sigma_{i-1}^{m_x} \left[\frac{\partial T_i}{\partial x_i} \right]$. The shape of the reinforcement corrosion is determined so as to minimize the value of this gradient, i.e., the computed temperature is close to the target temperature at the observation point. It is too difficult to obtain the appropriate shape for the reinforcement corrosion directly such that the computed temperature is close to the target temperature. In general, the appropriate shape is therefore computed by using the iterative method.

In this study, the steepest descent method is introduced to update the shape of the reinforcement

corrosion, and the step length is updated by the Sakawa-Shindo method (Sakawa *et al.* 1980). The update equation is shown as

$$\{x_i^{(l+1)}\} = \{x_i^{(l)}\} - [W^{(l)}]^{-1} \left\{ \int_{t_0}^{t_f} \frac{\partial J^*}{\partial x_i} dt \right\}^{(l)} \quad \text{on } \Gamma_{cont.} \quad (12)$$

where l and $[W]$ indicate the number of iterations and the diagonal matrix by the weighting parameter, and the inverse value of the weighting parameter W indicates the step length in the iterative computation.

The algorithm of the iterative computation is shown below.

1. Set of the number of iteration $l=1$ and the initial coordinates $\{x_i^{(l)}\}$, the convergence criterion ε .
2. Computation of the state equation (Eq. (8)).
3. Computation of the performance function $J^{(l)}$ (Eq. (5)).
4. Computation of the adjoint equation (Eq. (9)) and computation of the gradient of the Lagrange function with respect to the coordinates (Eq. (11)).
5. Update of shape of the reinforcement corrosion (Eq. (13)).
6. Check for the convergence; if $|J^{(l+1)} - J^{(l)}| < \varepsilon$ then stop, else go to step 7.
7. Computation of the state equation (Eq. (8)).
8. Computation of the performance function $J^{(l+1)}$ (Eq. (5)).
9. Update of weighting parameter; if $J^{(l+1)} < J^{(l)}$ then $W^{(l+1)} = 0.9W^{(l)}$ and go to step 4, else $W^{(l+1)} = 2.0W^{(l)}$ and go to step 5.

In addition, if the iterative computation¹⁾ for the state and the adjoint equations does not converge, the weighting parameter W is updated to $2.0W$, and the computation returns to the step 5.

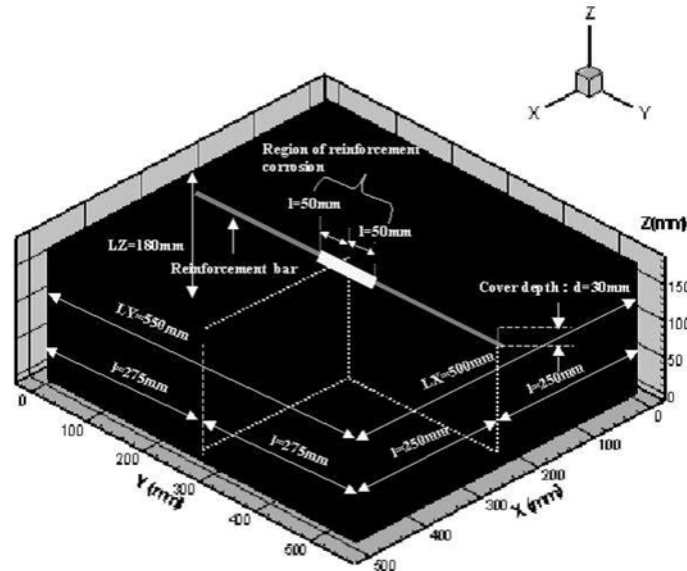


Fig. 5 Computational model (length of reinforcement corrosion 100 mm, diameter of reinforcement bar 16 mm)

¹⁾ The iterative computation indicates the computation by the element-by-element conjugate gradient method.

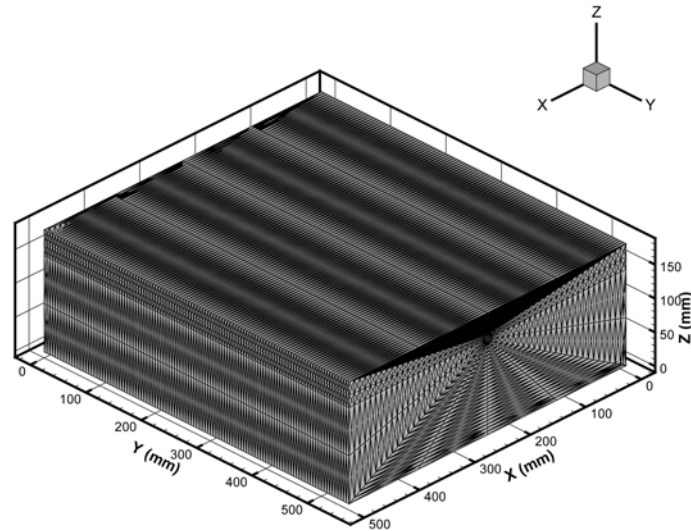


Fig. 6 Finite element mesh (Nodes : 242,000, Elements : 1,140,480)

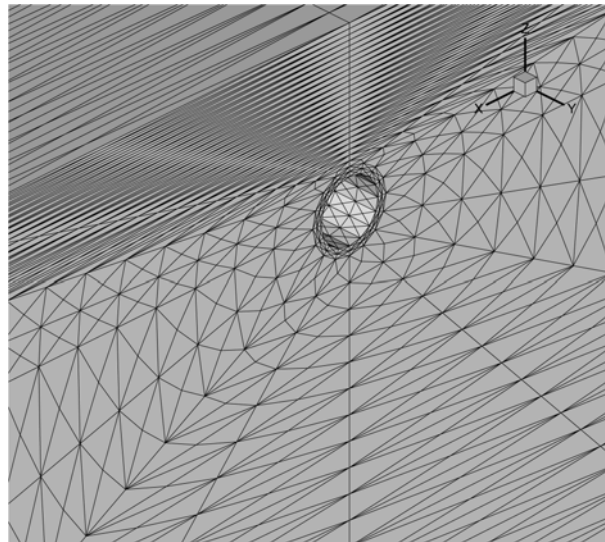


Fig. 7 Magnified figure around X=250 mm, Y=550 mm, Z=180 mm

5. Numerical experiments

In this study, the computational model shown in Fig. 5 is employed. The size of test piece is 500 mm×550 mm×180 mm and the diameter of the reinforcement bar is 16 mm. It is assumed that there is partial corrosion on the center of the reinforcement bar. The finite element mesh and the magnified figure around the reinforcement bar are shown in Figs. 6 and 7. The total number of nodes and elements are 242,000 and 1,140,480.

The computational conditions are shown in Table 1. In addition, the temperature boundary condition is given on the surface of the reinforcement bar. The temperature is given such as the Fig. 11 until

Table 1 Computational conditions

Real time (t_{max} sec.)	600
Convection coefficient (h W/m ² °C)	10.0
Ambient temperature (ϕ_{∞} °C)	21.3
Time of heating to steel (t_1 sec.)	240
Heat up ratio on surface of reinforcement bar (a °C/sec.)	0.081
Initial temperature in concrete ($\phi(t_0)$ °C)	19.5
Total number of nodes	242,000
Total number of elements	1,140,480
Time increment (Δt sec.)	5.0
Time steps	120
Convergence criterion ε	10^{-6}

Table 2 Physical constants

	Concrete	Reinforcement bar	Reinforcement corrosion
Density ρ (kg/m ³)	2.40×10^3	7.85×10^3	5.30×10^3
Specific heat c (J/kg °C)	1.15	4.70×10^{-1}	1.20
Thermal conductivity κ (W/m °C)	2.70	5.13×10^1	6.97×10^{-2}

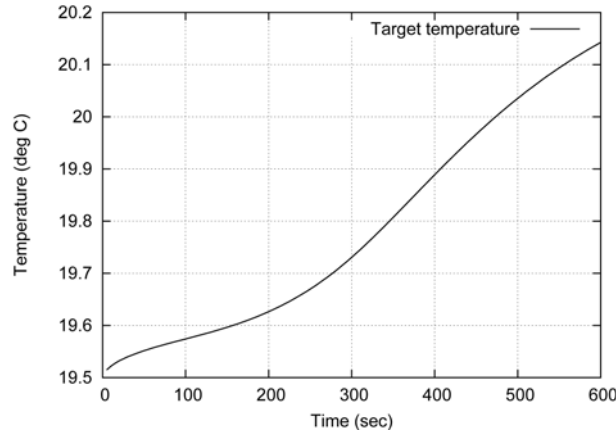


Fig. 8 Time history of temperature at observation point X=0.250 m, Y=0.275 m, Z=0.180 m (Target value)

T=240 sec., and the Neumann boundary condition, i.e., the heat flux is equal to zero, is given on the boundary after T=240 sec. (Eq. (13)). The boundary condition shown in Eq. (14) is given on the concrete surface. The observation point is set at the point, X=250 mm, Y=275 mm, Z=180 mm. The weighting diagonal matrix $[Q]$ is set 1.0 at the observation point, and is set 0.0 at the other points. In addition, the physical constants are shown in Table 2.

$$\begin{aligned} \phi &= at + \phi(t_0) \quad \text{on steel surface in } t \in [0, t_1] \\ q &= 0 \quad \text{on steel surface in } t \in [t_1, t_{max}] \end{aligned} \quad (13)$$

$$q = h(\phi - \phi_{\infty}) \quad \text{on concrete surface in } t \in [0, t_{max}] \quad (14)$$

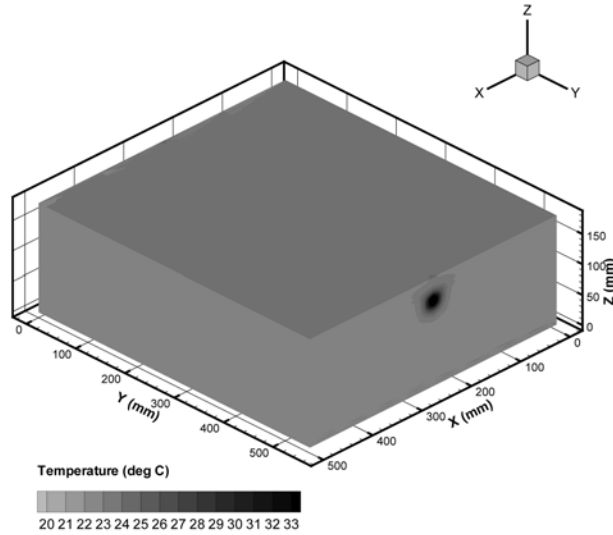


Fig. 9 Distribution of temperature at $t = 1$ in whole domain ($T=180$ sec.)

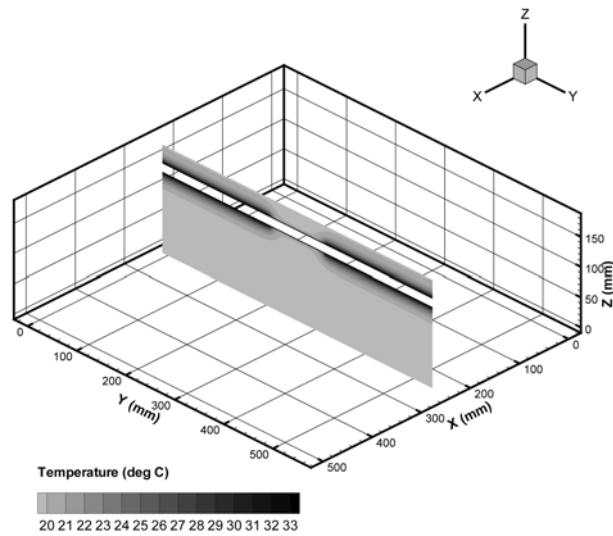


Fig. 10 Distribution of temperature at $t = 1$ on section $X=250$ mm ($T=180$ sec.)

5.1 Numerical example 1

It is assumed that the corrosion is uniformly distributed around the reinforcement bar. In addition, the length and the thickness of the reinforcement corrosion are set 100.0 mm and 1.0 mm. The heat transfer analysis based on FEM is carried out based on the above conditions. The computational result by the finite element analysis is shown in Fig. 8. It is seen that the temperature at the observation point gradually decreases. In this study, this result is used as an artificial observation data (Target value), and the inverse analysis is carried out. As the computational condition for the inverse analysis, the length and the thickness of the reinforcement corrosion at the iteration are given as 100.0 mm and 2.0 mm.

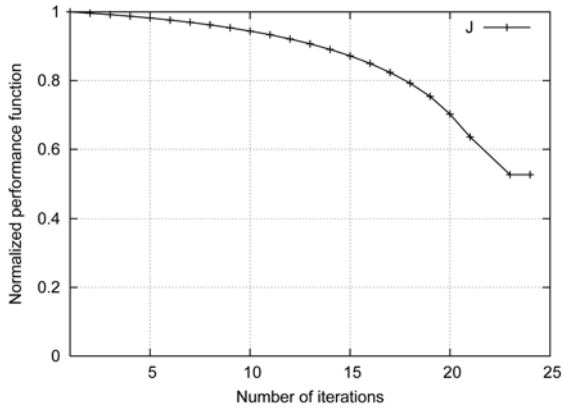


Fig. 11 Variation of performance function

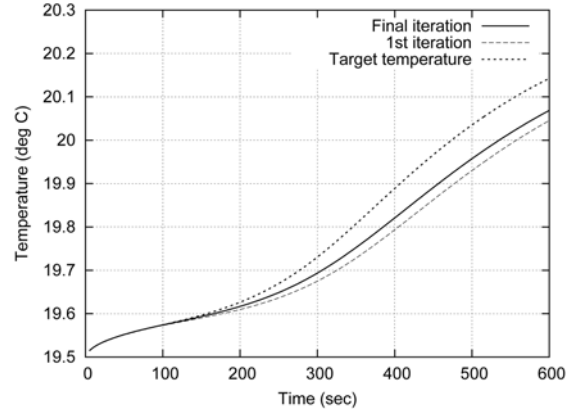


Fig. 12 Time history of temperature at observation point

Table 3 Comparison of volume for reinforcement corrosion

	Volume (mm ³)
Result at first iteration	9,391
Result at final iteration	8,560
Target value	4,708

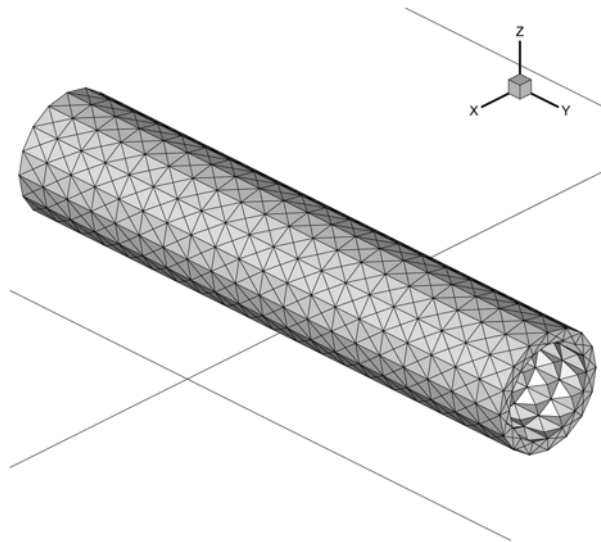


Fig. 13 Initial shape of reinforcement corrosion

The computational results at the first iteration are shown in Figs. 9 and 10. Fig. 9 and Fig. 10 show the contour figure of temperature in the whole domain and that on the section X=250 mm. It is seen that the temperature storage in the region of the reinforcement corrosion and transfer from the region without the reinforcement corrosion. Though, the appropriate temperature distribution is obtained, there is difference between the computed temperature and the target value. Therefore, the inverse analysis is carried out to obtain the appropriate shape of the reinforcement corrosion such that the

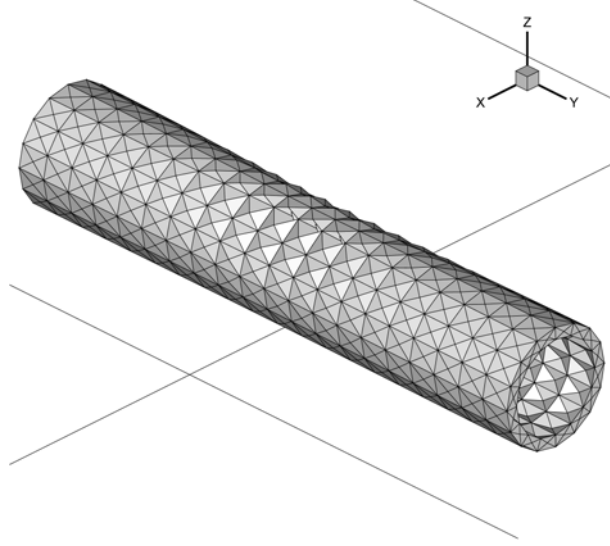


Fig. 14 Final shape of reinforcement corrosion

computed temperature is close to the target temperature at the observation point. Fig. 11 shows the variation of the performance function. It is found that the value of the performance function gradually decreases and converges. Fig. 12 shows the time history of the temperature at the observation point. The solid line indicates the computational result at the final iteration, and the dot and broken lines indicate the target temperature and the computational result at the first iteration. It is seen that the temperature at the final iteration is close to the target temperature comparing with the result at the first iteration. Figs. 13 and 14 show the shape of the reinforcement corrosion at first and the final iterations. The center region of the final shape hollows comparing with that of the first iteration. In addition, Table 3 shows the comparison of the volume for the reinforcement corrosion. It is found that the result at the final iteration is close to the target value comparing with the result at the first iteration, however there is difference between the result at the final iteration and the target value. Therefore, it is necessary to improve the computational algorithm such that the final shape can be much more close to the target shape.

5.2. Numerical example 2

The previous result indicates that even if the thickness for the reinforcement corrosion is uniform, the computed corrosion thickness is not uniform. Because the distribution of the gradient vector $\left\{\frac{\partial J}{\partial x_i}\right\}$ depends on the position of the observation point, the value of the gradient vector $\left\{\frac{\partial J}{\partial x_i}\right\}$ can not be uniformly obtained. Therefore, the formulation with respect to the gradient vector $\left\{\frac{\partial J}{\partial x_i}\right\}$ is improved such that the gradient is distributed a concentric circle. First of all, the gradient vectors $\left\{\frac{\partial J}{\partial x}\right\}$ and $\left\{\frac{\partial J}{\partial z}\right\}$ are expressed by the polar coordinate system (Eq. (15)).

$$\begin{aligned}\frac{\partial J^*}{\partial x_i} \delta x_i &= \frac{\partial J^*}{\partial x} \delta x + \frac{\partial J^*}{\partial y} \delta y + \frac{\partial J^*}{\partial z} \delta z = \frac{\partial J^*}{\partial y} \delta y + \left(\frac{\partial J^*}{\partial x} \frac{\partial x}{\partial r} + \frac{\partial J^*}{\partial z} \frac{\partial z}{\partial r}\right) \delta r + \left(\frac{\partial J^*}{\partial x} \frac{\partial x}{\partial \theta} + \frac{\partial J^*}{\partial z} \frac{\partial z}{\partial \theta}\right) \delta \theta \\ &= \frac{\partial J^*}{\partial y} \delta y + \frac{\partial J^*}{\partial r} \delta r + \frac{\partial J^*}{\partial \theta} \delta \theta\end{aligned}\tag{15}$$

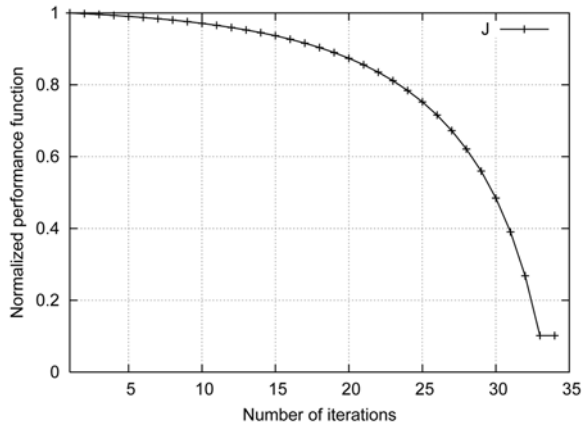


Fig. 15 Variance of performance function

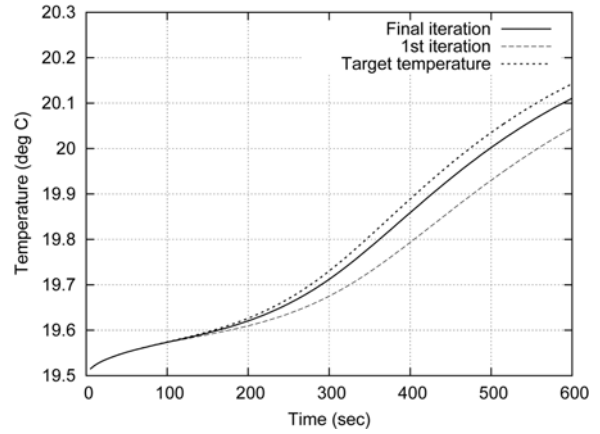


Fig. 16 Time history of temperature at the observation point

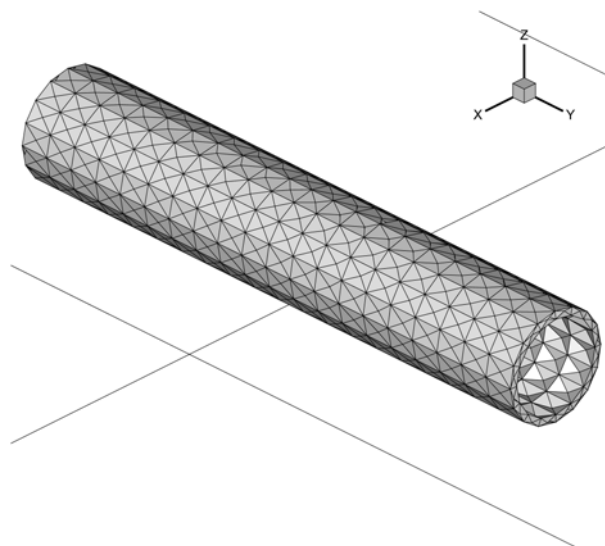


Fig. 17 Final shape of reinforcement corrosion

Table 4 Comparison of computational results (Initial length of reinforcement corrosion 100 mm)

	Volume (mm ³)	Thickness of corrosion (mm)	Length of corrosion (mm)
Result at first iteration	9,391	2.00	100.00
Result at final iteration	4,980	1.26	100.00
Target value	4,708	1.00	100.00

If the gradient is distributed a concentric circle, this fact indicates the gradient does not vary for the θ direction, and $\delta\theta$ is equal to zero. Therefore, Eq. (15) can be represented as

$$\frac{\partial J^*}{\partial x_i} \delta x_i = \frac{\partial J^*}{\partial y} \delta y + \frac{\partial J^*}{\partial r} \delta r = \frac{\partial J^*}{\partial y} \delta y + \left(\frac{\partial J^*}{\partial x} \frac{\partial x}{\partial r} + \frac{\partial J^*}{\partial z} \frac{\partial z}{\partial r} \right) \delta r = \frac{\partial J^*}{\partial y} \delta y + \left(\frac{\partial J^*}{\partial x} \cos \theta + \frac{\partial J^*}{\partial z} \sin \theta \right) \delta r \quad (16)$$

In addition, even if the gradient distribution is obtained by the Eq. (16), the gradient $\left\{ \frac{\partial J}{\partial r} \right\}$ does not uniformly distribute for the r direction. Therefore, the average value for the gradient $\left\{ \frac{\partial J}{\partial r} \right\}$ is calculated, and the value is employed to move the nodal position on the surface of corrosion.

The computational results are shown as follows. Figs. 15 and 16 show the variation of the performance function and the time history of the temperature at the observation point. It is seen that the converged value of the performance function is less than that of the previous study, and the computed temperature at the final iteration can be much more close to the target temperature comparing with the result of the previous study. The final shape of the reinforcement corrosion is shown in Fig. 17. It is found that the thickness of the corrosion is thinner than that obtained in the

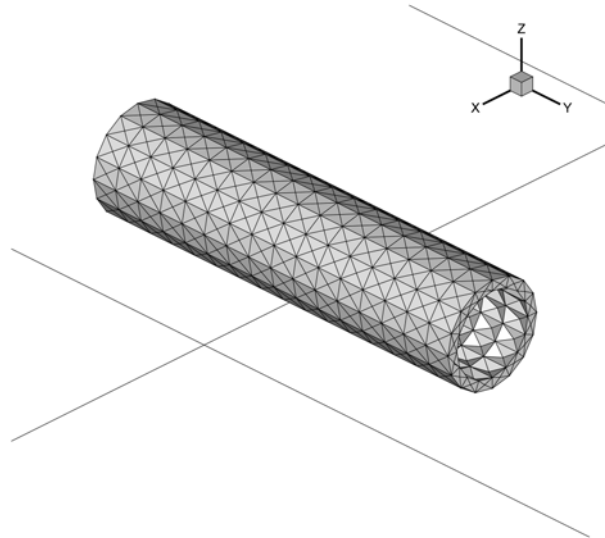


Fig. 18 Initial shape of reinforcement corrosion (initial length : 80 mm)

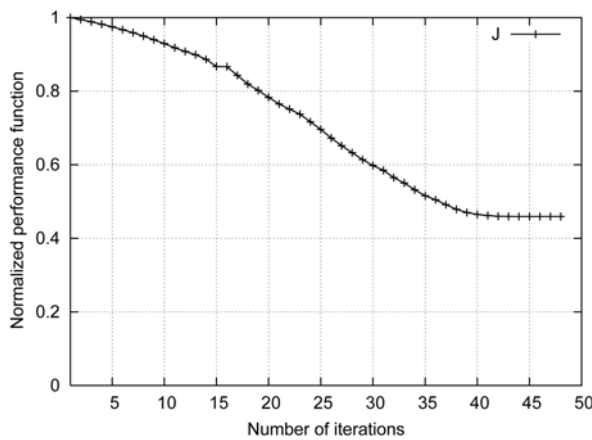


Fig. 19 Variation of performance function

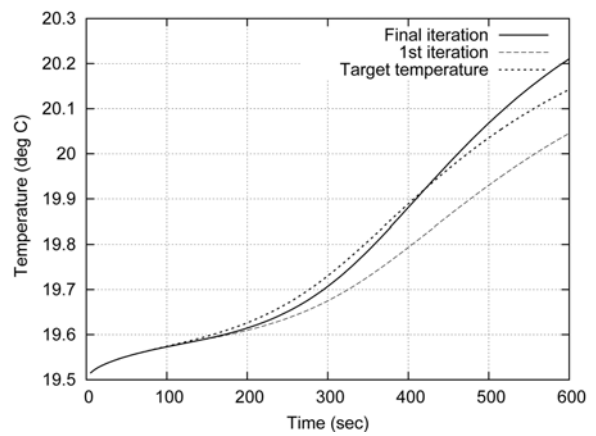


Fig. 20 Time history of temperature at observation point

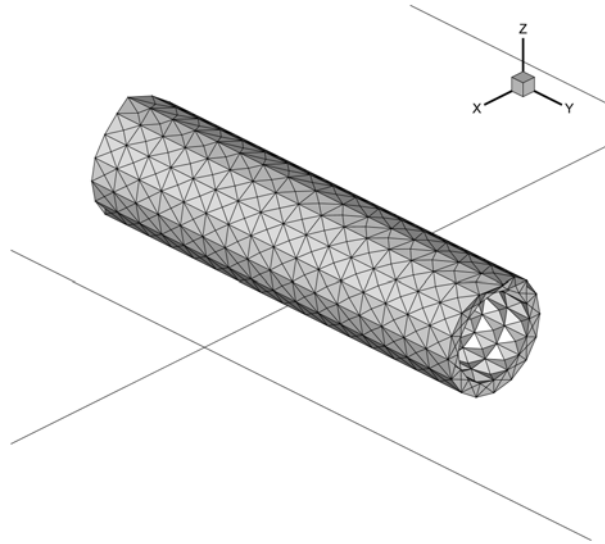


Fig. 21 Final shape of reinforcement corrosion (initial length : 80 mm)

Table 5 Comparison of computational results (Initial length of reinforcement corrosion 80 mm)

	Volume (mm ³)	Thickness of corrosion (mm)	Length of corrosion (mm)
Result at first iteration	7,513	2.00	80.00
Result at final iteration	9,251	2.34	84.39
Target value	4,708	1.00	100.00

previous study. Table 4 shows the comparison of the volume, the thickness and the length for the corrosion. The length of the corrosion is calculated by the difference between the maximum and the minimum values for the Y-axis. It is found that the volume and the thickness of the corrosion at the final iteration are close to the target volume. In addition, the length of the corrosion did not completely vary in the iterative computation.

5.3. Numerical example 3

In this examination, the dependency for the initial length of the corrosion is investigated. The initial thickness and the initial length of the corrosion are set 2.0 mm and 80.0 mm. Fig. 18 shows the initial shape of the reinforcement corrosion. The computational results are shown as follows. Fig. 19 shows the variation of the performance function. It is found that the convergence rate is slower than that of the previous cases. In addition, Fig. 20 shows the time history of the temperature at the observation point. It is seen that though the computed temperature is higher than the target value near the terminal time, the computed temperature is totally good agreement with the target value. Fig. 21 shows the final shape of the reinforcement corrosion. Though the top of the shape for the reinforcement corrosion is extended, the other nodes was not updated for Y-direction. Table 5 shows the comparison of the volume, the thickness and the length for the corrosion. It is found that the computational results at the final iteration are not good

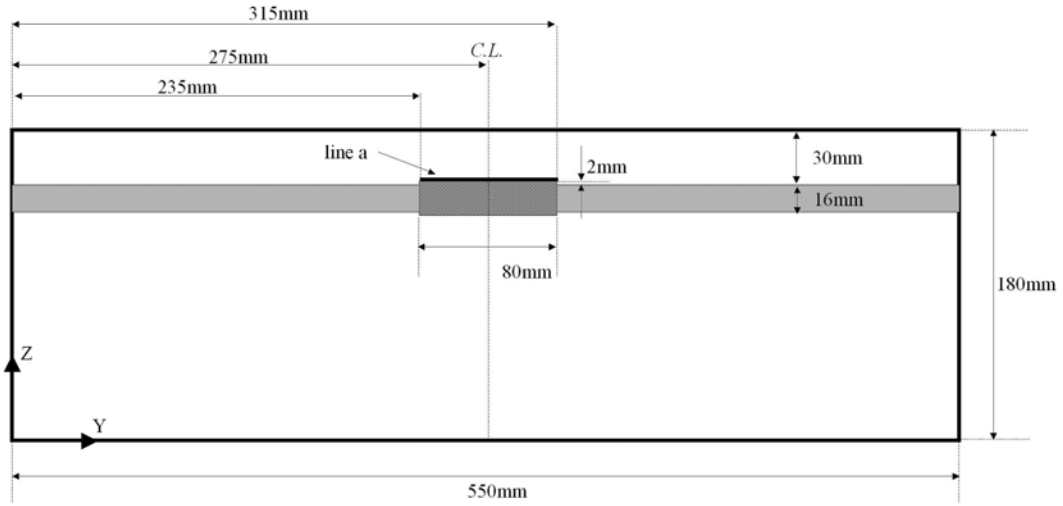


Fig. 22 Cross sectional figure on surface of X=250 mm and initial condition for shape determination problem

Table 6 Computational conditions for observation points

Case	Numbr of observation points	Position of observation points
A	1	Y=275 mm
B	2	Y=250 mm, 300 mm
C	5	Y=225 mm, 250 mm, 275 mm, 300 mm, 325 mm

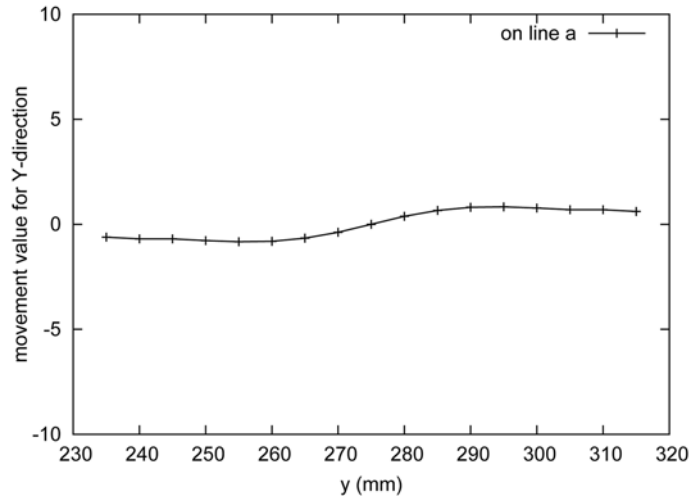


Fig. 23 Distribution of movement value $\left(-W^{-1} \int_{t_0}^{t_f} \frac{\partial J}{\partial y} dt\right)$ for Y axis (Case A : one observation point)

agreement with the target value. Therefore, it appears that the initial length of the reinforcement corrosion should be given the appropriate length estimated by the heat image.

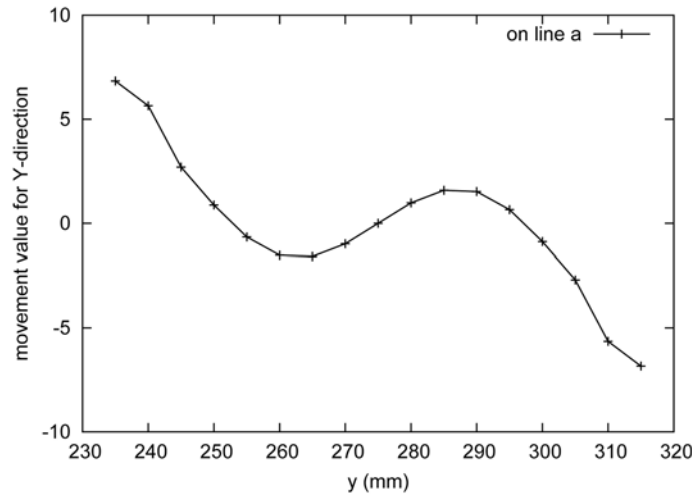


Fig. 24 Distribution of movement value $\left(-W^{-1} \int_{t_0}^{t_j} \frac{\partial J^*}{\partial y} dt\right)$ for Y axis (Case B : two observation points)

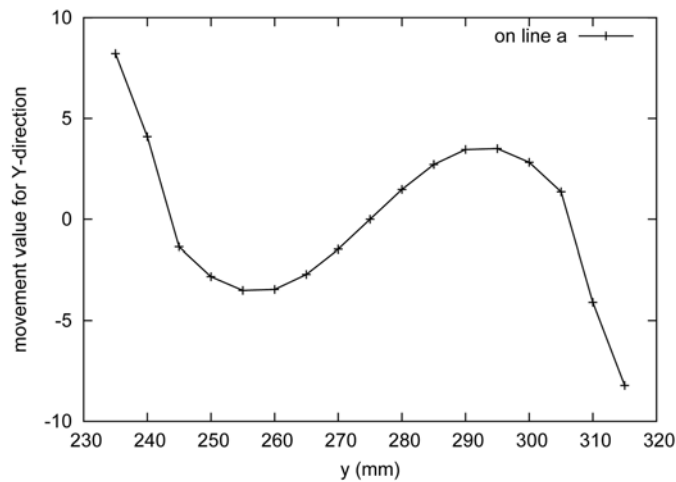


Fig. 25 Distribution of movement value $\left(-W^{-1} \int_{t_0}^{t_j} \frac{\partial J^*}{\partial y} dt\right)$ for Y axis (Case C : five observation points)

5.4 Remarks for the number of observation points

In this section, an examination is carried out to investigate the method that the appropriate corrosion shape is obtained in case of numerical example 3. The computational model used in the numerical example 3 is employed, and the dependency for the number of observation points is investigated. The computational conditions are shown in Fig. 22 and Table 6.²⁾ The observation points are set on the line X=250 mm and Z=180 mm, and the weighting parameter W is set 1.0.

The distribution of movement value for Y-direction at the first iteration is shown in Figs. 23-25.

²⁾Case A" is the same condition as numerical example 3.

The distribution shows the distribution of the movement value $\left(-w^{-1} \int_0^t \frac{\partial J}{\partial y} dt\right)$ on the line a (See Fig. 22). Fig. 23 shows the distribution of the movement value for Y-direction in case that one observation point is employed. It is found that appropriate movement value is obtained such that the corrosion is expanded for Y-direction comparing to the initial state. In addition Figs. 24 and 25 show the distribution of the movement value for Y-direction in case that two and five observation points are employed. It is seen that the sign of the movement value $\left(-w^{-1} \frac{\partial J}{\partial y}\right)$ on the line a is changed in the sections “235 mm \leq Y \leq 275 mm” and “275 mm \leq Y \leq 315 mm”. In these sections, the value of the same sign should be obtained, because the direction for the movement of the nodal points are same direction. Therefore, it is found that there is a case that the appropriate gradient distribution is not obtained, even if the number of the observation points are increased.

6. Conclusions

In this paper, the numerical shape determination system of the 3-D reinforcement corrosion in concrete based on the observed temperature on the concrete surface was presented, and some numerical experiments were shown. To simulate the heat transfer field, the heat transfer equation was introduced, and the finite element method was applied. The adjoint variable method is employed to determine the shape of the 3-D reinforcement corrosion. The iterative computation was carried out by using the steepest descent method, and the weighting parameter was updated based on the method proposed by Sakawa *et al.*

In the numerical experiments, the shape of the reinforcement corrosion was determined such that the computed temperature is close to the target temperature at the observation point. In this study, the computed result is employed as the target temperature. The computed result is finally obtained, and the computed temperature could be close to the target temperature comparing with the temperature at the first iteration. However, comparing the volume between the final shape and the target shape, it was found that the final result is not close to the target result. Therefore it can be said that it is necessary to improve the computational algorithm to be able to obtain the much more accurate result. In this study, the restrict condition that the nodes on the corrosion surface move to the radius r and the angle θ directions was introduced to solve this problem. Finally, the final shape could be close to the target shape comparing with the result of the previous examination. As the next investigation, this model was applied to the problem that the shorter initial length than that of the target shape is given. Consequently, though the computed temperature was close to the target temperature, the final shape was not good agreement with the target shape. In addition, it was found that it is not usual that the appropriate movement value is obtained, even if the number of the observation point is increased. Therefore, it appears that it is necessary to give the initial length of the reinforcement corrosion based on the result of the heat image analysis.

Acknowledgments

I wish to thank the staff at the Research Institute for Information Technology, Kyushu University, enabling me to use the super computer system.

References

- Azegami, H. and Takeuchi, K. (2006), "A smoothing method for shape optimization: traction method using the robin condition", *Int. J. Comput. Meth.*, **3**(1), 21-33.
- Bostock, M.G. (2002), "Kirchhoff-approximate inversion of teleseismic wavefields", *Geo. J. Int.*, **149**, 787-795.
- Challis, Vivien J. and Guest, James K. (2009), "Level set topology optimization of fluids in stokes flow", *Int. J. Numer. Meth. Eng.*, **79**, 1284-1308.
- Dimet, F.X.L., Navon, I.M. and Daescu, D.N. (2002), "Second order information in data assimilation", *Mon. Weather Rev.*, **130**(3), 629-648.
- Gunzburger, M.D., Hou, L.S., Manservigi, S. and Yan, Y. (1998), "Computation of optimal controls for incompressible flow", *Int. J. Comput. Fluid Dyn.*, **11**, 181-191.
- He, J.W., Glowinski, R., Metacalfe, R. and Periaux, J. (1998), "A numerical approach to the control and stabilization of advection-diffusion systems: application to viscous drag reduction", *Int. J. Comput. Fluid Dyn.*, **11**, 131-156.
- Jameson, A. and Kim, S. (2003), "Reduction of the adjoint gradient formula in the continuous limit", 41st AIAA Aero. Sci. Meet., AIAA 2003-0040.
- Khalaj-Amirhosseini, M., Hodjat-Kashani, F. and Kamarei, M. (2008), "Reconstruction of the shape and location of arbitrary homogeneous objects using sequentially incidences", *Microw. Opt. Techn. Let.*, **50**(5), 1248-1251.
- Kreibig, R., Benedix, U., Gorke, U.J. and Lindner, M. (2007), "Identification and estimation of constitutive parameters for material laws in elastoplasticity", *GAMM-Mitt.*, **30**(2), 458-480.
- Langenberg, K.J. (1989), "Introduction to the special issue on inverse problem", *Wave Motion*, **11**, 99-112.
- Luo, Zhen and Tong, Liyong (2008), "A level set method for shape and topology optimization of large-displacement compliant mechanism", *Int. J. Numer. Meth. Eng.*, **76**, 863-892.
- Ogawa, Y. and Kawahara, M. (2003), "Shape optimization of body located in incompressible viscous flow based on optimal control theory", *Int. J. Comput. Fluid Dyn.*, **17**(4), 243-251.
- Pironneau, O. (1973), "On optimum profiles in stokes flow", *J. Fluid Mech.*, **59**(1), 117-128.
- Pironneau, O. (1974), "On optimum design in fluid mechanics", *J. Fluid Mech.*, **64**(1), 97-110.
- Sakawa, Y. and Shindo, Y. (1980), "On global convergence of an algorithm for optimal control", *IEEE T. Automat. Contr.*, **ac-25**(6), 1149-1153.
- Taniguchi, O., Shigematsu, B., Horie, H. and Oshita, H. (2008), "Application of thermography to detection of internal defects in reinforced concrete by heat charge due to electromagnetic induction", *J. JSCE(E)*, **64**(1), 173-185.
- Yagi, H. and Kawahara, M. (2007), "Optimal shape determination of a body located in incompressible viscous fluid flow", *Comput. Method. Appl. M.*, **196**(49), 5084-5091.